

Study on electromagnetic interference and shielding efficiency of power grid on-line elimination equipment

Xuejun Fan^{1,2}, Yang Li¹, Yongliang Li^{1,2}, Tong Li^{1*}, Lijie Yin¹, Keke Yan¹

¹State Grid Handan Power Supply Company, Handan 056004, China;

²Hebei Smart Grid Power Distribution Operation and Maintenance Technology Innovation Center, Handan 056004, China;

Abstract. The robot-based automatic power grid defect elimination device represents the future direction of power grid inspection and defect elimination devices. However, the presence of strong electromagnetic interference in the vicinity of power grids poses potential risks to the application of automatic defect elimination devices. This study initially conducts theoretical analysis and calculations to analyse the spatial distribution of electromagnetic fields around 220kV 100MW high-voltage lines in a power grid. The results indicate that electric field intensity can exceed 70kV/m in areas near these high-voltage lines. Subsequently, electromagnetic fields within the operational range of the elimination device are simulated and analysed, leading to selection and optimization of shielding materials and structures. When non-metallic insulating materials are used, equipment is fully exposed to the power grid's electromagnetic field, making internal devices susceptible to interference; however, employing metal aluminum materials achieves better shielding effects. A continuous metal shielding layer effectively shields against electric fields, while openings or gaps in the shell lead to deteriorated shielding performance. These findings demonstrate that appropriate selection of shielding materials and suitable structural design are crucial factors for achieving excellent shielding effects. To ensure both safety and efficient electromagnetic shielding, a multi-layer composite shielding structure is necessary for power grid elimination devices. Overall, these analysis results provide valuable guidance for designing, operating, and maintaining such devices.

1 Introduction

In the long-term operation of the power transmission system, certain "defects" are inevitable, such as loose bolts and dislodged pins, which pose a risk to the network operation. The traditional manual approach to addressing these "defects" is inefficient and carries inherent risks. Therefore, there is a desire to replace manual intervention with robotic solutions for the elimination of these "defects".

The current development direction for robots is to replace manual power grid inspection and maintenance. However, there are several issues that need to be studied, one of which is the impact of electromagnetic interference from the power grid on robot electronic equipment. The online defect elimination robot operates in a suspension mode, directly suspended on high-voltage cables during work and coming into direct contact with power grid devices during the elimination operation. Due to factors such as climate and workload, the distribution of electromagnetic fields around the power grid is complex, which may lead to image recognition errors, mis-actions, communication failures, and even permanent damage to the power grid elimination robot in severe cases. Therefore, it is essential to study the distribution of electromagnetic fields within the working range of the power grid elimination robot and its impact on the robot in complex electromagnetic field environments.

Researchers have proposed various methods for the analysis and calculation of electric grid electromagnetic fields. In the 1950s, American scholar Leonard B. Loeb utilized the analog charge method to calculate the distribution of electric fields [1] from different types of electrodes to the ground. In the 1990s, scholars such as Krajewski W used the moment method to calculate [2] the electric field distribution near 400kV power grid transmission lines. In 2009, M. Trlep et al. employed the finite element method to analyze [3] the electric field distribution when conductors were under high-voltage power grids. Furthermore, in 2015, Wang Jingxiao, Gao Yanxia and other scholars from Shenzhen University proposed a two-dimensional numerical analysis and calculation method using analog charge and mirror charge for electric fields[4]. Lastly, in 2019, Wang Xuxu, Li Xin and other scholars from Chongqing University introduced a method that combines simulated charge with finite element analysis to calculate [5] the three-dimensional electric field distribution of high-voltage electrical equipment.

The near-field electromagnetic field of high-voltage transmission lines is analyzed in this paper using the simulated charge method and BioSavart's theorem. The analysis reveals that the maximum magnetic field strength in the near-field area is 10Gs, with the highest electric field reaching 70kV/m, highlighting the need for focusing on electric field shielding. Subsequently, a three-dimensional electromagnetic field analysis was conducted using CST electromagnetic simulation

analysis software. Based on the analysis results, the device structure was optimized to reduce internal electric field intensity to less than 5V/m, thereby achieving improved shielding effectiveness. The power grid defect elimination device is susceptible to external electromagnetic field interference during operation, leading to issues such as image distortion, control failure, and communication failure. By utilizing the analysis method proposed in this paper, the source of electromagnetic interference can be effectively identified and corresponding improvement methods can be suggested to enhance the reliability of the device's operation.

2 Field Numeric Calculation

2.1 Theoretical calculation of near-field electric field of power grid

For the calculation of the electric field, the analog charge method is utilized in this study. The high-voltage cable is considered equivalent to an analog charge, with its position representing the vertical cross-section of the high-voltage cable (as illustrated in Figure 1). Let Q be the equivalent charge of the high-voltage cable. Since the ground surface potential is 0, for ease of calculation, we set Q_4, Q_5, Q_6 as its mirror equivalent charge. Therefore, we can establish the following three equations: $Q_1, Q_2, Q_3, Q_4, Q_5, Q_6$.

$$\begin{cases} P_{11}Q_1 + P_{12}Q_2 + \dots + P_{16}Q_6 = \varphi_{M1} \\ P_{21}Q_1 + P_{22}Q_2 + \dots + P_{26}Q_6 = \varphi_{M2} \\ P_{31}Q_1 + P_{32}Q_2 + \dots + P_{36}Q_6 = \varphi_{M3} \end{cases} \quad (1)$$

Since, \dots is the opposite of, and, the equality sign, equation (1) can be simplified as follows:

$$\begin{cases} P'_{11}Q_1 + P'_{12}Q_2 + P'_{13}Q_3 = \varphi_{M1} \\ P'_{21}Q_1 + P'_{22}Q_2 + P'_{23}Q_3 = \varphi_{M2} \\ P'_{31}Q_1 + P'_{32}Q_2 + P'_{33}Q_3 = \varphi_{M3} \end{cases} \quad (2)$$

Where P'_{ij} is the potential coefficient: $P'_{ij} = \frac{1}{2\pi\epsilon_0} \ln\left(\frac{r'_{ij}}{r_{ij}}\right)$, $i, j = 1, 2, 3$; i denote the calculated point for the known potential, j is the analog charge, j' represents the mirror charge of the analog charge j , and r_{ij} represents the distance between j and i .

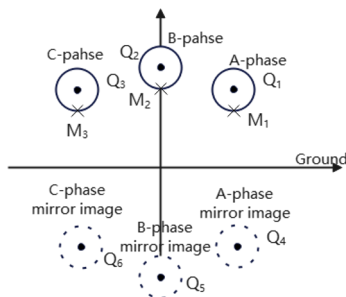


Fig. 1. The equivalent point for charge simulation method

In this case, the potential position is chosen as the regional potential near the high-voltage cable, which can

be considered approximately equivalent to the high-voltage cable potential. By solving the aforementioned equations, we can obtain the simulated charge Q . Subsequently, the electric field at any point in space $M(x, y)$ can be characterized by the following formula:

$$\begin{aligned} \vec{E}_x &= \sum_{i=0}^k E_{ixR} + \sum_{i=0}^k E_{ixI} = E_{xR} + jE_{xI} \quad (3) \\ \vec{E}_y &= \sum_{i=0}^k E_{iyR} + \sum_{i=0}^k E_{iyI} = E_{yR} + jE_{yI} \end{aligned}$$

k is the number of simulated charges, E_{ixR} represents the real part of the electric field at point M along the x axis, while the imaginary part E_{ixI} can be expressed as:

$$\begin{aligned} E_{ixR} &= -\frac{\partial\varphi_R}{\partial x} = \frac{Q_{iR}}{2\pi\epsilon_0} \left(\frac{x_0 - x_i}{r_i^2} - \frac{x_0 - x_i}{r_i'^2} \right) \\ E_{ixI} &= -\frac{\partial\varphi_I}{\partial x} = \frac{Q_{iI}}{2\pi\epsilon_0} \left(\frac{x_0 - x_i}{r_i^2} - \frac{x_0 - x_i}{r_i'^2} \right) \quad (4) \\ E_{iyR} &= -\frac{\partial\varphi_R}{\partial y} = \frac{Q_{iR}}{2\pi\epsilon_0} \left(\frac{y_0 - y_i}{r_i^2} - \frac{y_0 - y_i}{r_i'^2} \right) \\ E_{iyI} &= -\frac{\partial\varphi_I}{\partial y} = \frac{Q_{iI}}{2\pi\epsilon_0} \left(\frac{y_0 - y_i}{r_i^2} - \frac{y_0 - y_i}{r_i'^2} \right) \end{aligned}$$

The coordinates of medium and high voltage cables are, $P_i(x_i, y_i)$, $i = 1, 2, 3$; r_i is the distance from wire i to field point P , r_i' is the distance from the mirror image of wire i to field point P , and $r_i^2 = (x_0 - x_i)^2 + (y_0 - y_i)^2$, $r_i'^2 = (x_0 - x_i')^2 + (y_0 - y_i')^2$.

Then the resultant field strength of point P is:

$$\begin{aligned} \vec{E} &= (E_{xR} + jE_{xI})\vec{e}_x + (E_{yR} + jE_{yI})\vec{e}_y \\ &= E_x\vec{e}_x + E_y\vec{e}_y \end{aligned} \quad (5)$$

$$E_x = \sqrt{E_{xR}^2 + E_{xI}^2} \quad E_y = \sqrt{E_{yR}^2 + E_{yI}^2}$$

2.2 Theoretical calculation of near-field magnetic field of power grid

The Biot-Savart Law describes the magnetic induction intensity B generated by a current element at any point P in space under steady state. The magnitude of the magnetic induction dB generated by the current element at a point P in space is directly proportional to the size of the current element, as well as to the sine of the angle between the position vector and the current element from the current element to point P , and inversely proportional to the square of the distance from the current element to point P [6-7]. Its equation is given by:

$$d\vec{B} = \frac{\mu_0 I dl \times d\vec{r}}{4\pi r^3} = \frac{\mu_0 I dl \sin\theta}{4\pi r^2} \quad (6)$$

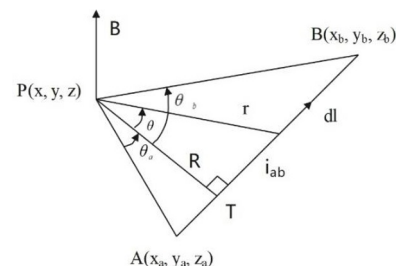


Fig. 2. Magnetic field generated by the carrier at any point in space

Where, as shown in Fig. 2, I is the excitation current, dl is the current element, and μ_0 is the vacuum permeability. \vec{r} is the direction vector from the current element to point P .

According to Biot-Savart's law, the magnetic field generated by a continuous carrier fluid in space from the start point $A(x_a, y_a, z_a)$ to the end point $B(x_b, y_b, z_b)$ can be characterized by the following formula:

$$\vec{B} = \frac{\mu_0 i_{ab}}{4\pi} \int_A^B \frac{dl \times r_0}{r^2} \quad (7)$$

Where \hat{l}_{ab} is the fluid carrying current r_0 and is the vector unit of the current element microsegment dl pointing to point P ; μ_0 is the air magnetic permeability; r is the distance from dl to point P .

The above formula is derived from a transformation of geometric relations.

$$\vec{B} = \frac{\mu_0 i_{ab}}{4\pi R} (\sin \theta_a + \sin \theta_b) \quad (8)$$

$$\sin \theta_a + \sin \theta_b = \frac{l_{AT}}{l_{PA}} + \frac{l_{AB} - l_{AT}}{l_{PB}} \quad (9)$$

The direction of magnetic field \vec{B} is

$$\vec{e}_B = \vec{e}_{AB} \times \vec{e}_{PB} = \frac{\vec{l}_{AB} \times \vec{l}_{PB}}{|\vec{l}_{AB} \times \vec{l}_{PB}|} \quad (10)$$

$$\vec{l}_{1+B} \times \vec{l}_{PB} = \begin{vmatrix} e_x & e_y & e_z \\ x_b - x_a & y_b - y_a & z_b - z_a \\ x - x_b & y - y_b & z - z_b \end{vmatrix} \quad (11)$$

Where e_x, e_y, e_z are unit vectors on x, y, z direction respectively.

2.3 Numerical calculation

The three-phase current flowing through a high-voltage cable is a symmetrical sinusoidal current, and the voltage and current can be characterized by an effective phasor. The phase voltage of a high-voltage cable can be expressed as follows:

$$\begin{aligned} \dot{U}_A &= U_{AR} + jU_{AI} \\ &= |U_A| \cos \theta + j|U_A| \sin \theta \end{aligned} \quad (12)$$

$$\begin{aligned} \dot{U}_B &= U_{BR} + jU_{BI} \\ &= |U_B| \cos(\theta + 2\pi/3) + j|U_B| \sin(\theta + 2\pi/3) \end{aligned}$$

$$\begin{aligned} \dot{U}_C &= U_{CR} + jU_{CI} \\ &= |U_C| \cos(\theta - 2\pi/3) + j|U_C| \sin(\theta - 2\pi/3) \end{aligned}$$

Current can be expressed as:

$$\begin{aligned} \dot{I}_A &= I_{AR} + jI_{AI} \\ &= |I_A| \cos \theta + j|I_A| \sin \theta \end{aligned} \quad (13)$$

$$\begin{aligned} \dot{I}_B &= I_{BR} + jI_{BI} \\ &= |I_B| \cos(\theta + 2\pi/3) + j|I_B| \sin(\theta + 2\pi/3) \end{aligned}$$

$$\begin{aligned} \dot{I}_C &= I_{CR} + jI_{CI} \\ &= |I_C| \cos(\theta - 2\pi/3) + j|I_C| \sin(\theta - 2\pi/3) \end{aligned}$$

Taking a 220kV voltage 100MW rated transmission power single-loop three-phase triangulation two-split line as an example, the line laying parameters are illustrated in Figure 3 below. Due to the fact that the distance between the split wires is much smaller than the phase distance, the split wire can be considered equivalent to a center wire.

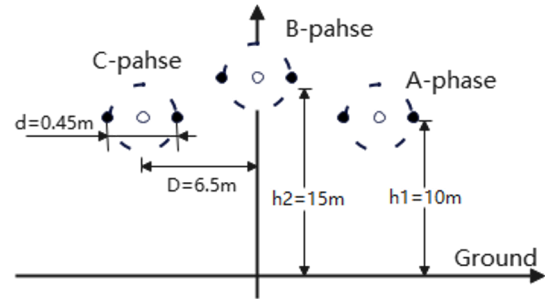


Fig.3. Structure parameters of 220kV power grid

Substituting the above formula into another formula, and conducting Matlab simulation and calculation, we obtained the distribution curve of two-dimensional electric field amplitude and magnetic induction intensity in the vicinity of the high-voltage cable, as shown in Fig. 4. The resulting electric field distribution forms a saddle-shaped curve around the symmetrical distribution of the center wire, with peak field intensity appearing directly below phase A and phase C of the high-voltage cable. The distribution of magnetic induction intensity also exhibits symmetrical characteristics around the center wire, with maximum value occurring directly below it before rapidly decaying towards outer areas[8-10].

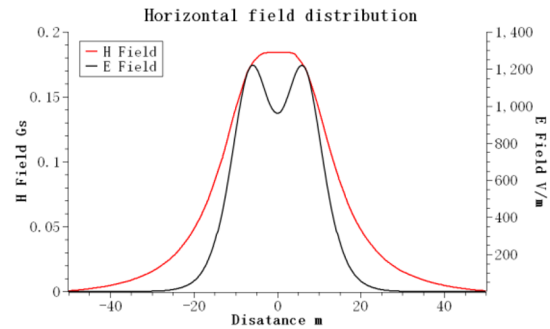


Fig.4. Field distribution curve at 1.5m above the ground

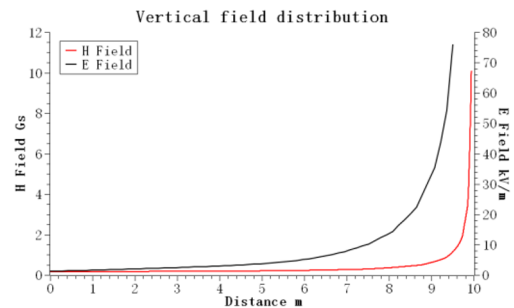


Fig.5. The field distribution in the vertical direction of the three-phase cable

Based on the results of numerical analysis, it is evident that there exists a significantly strong electric field in close proximity to the cable. The intensity of the

electric field near the high-voltage line can exceed 70kV/m, while the magnetic field intensity can also surpass 10Gs. The power grid elimination device is directly installed on the high-voltage cable, and improper handling of the strong electric field may lead to interference or even damage to the equipment. Therefore, it is imperative to analyze both the distribution of electric fields surrounding the surface and within the device under external interference from the high-voltage cable.

3 Analysis and optimization of electric field distribution

The online elimination device is primarily utilized for the automatic maintenance of power grid equipment, which includes the maintenance of bolts, pins, and other parts' status. It also involves inspections for power grid discharge, pollution, crushing, aging, and other related issues. The device operates using four driving wheels to control movement along the cable; two driving wheels are positioned on each side and mounted on two parallel equipotential cables of the split wire. These driving wheels are constructed from polytetrafluoroethylene material known for its excellent mechanical wear resistance, strength, and insulation performance. The simplified model of the elimination device can be seen in Fig. 6 below.

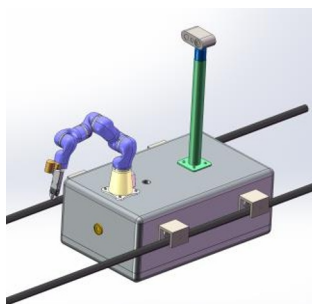


Fig.6. Structure diagram of power grid deficit elimination device

In the preceding section of this paper, the simulated charge method was utilized to calculate the boundary field distribution. However, it is challenging to analyze the influence of equipotential on the electric field distribution using this simple simulated charge method. Therefore, in the following section, finite element three-dimensional simulation analysis software will be employed for this purpose. The key factors to be taken into consideration include: a. the impact of different materials on the electric field distribution; b. magnetic shielding effect of material selection. All subsequent 3D simulation analyses are conducted using Dassault CST software. The limited modeling capability of simulation software necessitates the use of Solidworks for modeling, with the resulting model being subsequently imported into the simulation software.

When utilizing a non-metallic shell, such as an epoxy shell material in this instance, the potential of the split wire is set to 220kV. A reference point with a potential of 0 is established 15 meters below the split wire. The simulation results are depicted in Figure 7. In the vicinity of the high-voltage cable, the electric field strength is relatively high. The highest electric field strength near the surface of the high-voltage cable measures

approximately 3kV/m, while inside the shell it reaches 400V/m. The electric field near the central area tends towards zero. It should be noted that due to their metallic composition, screws at the bottom of both camera shell and camera bracket cause local distortion in electric field distribution near these components.

When a metal shell is utilized, the simulated material

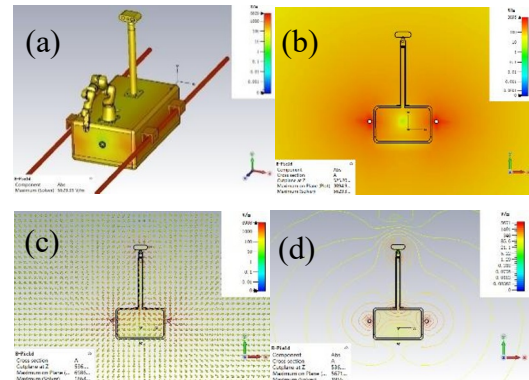


Fig.7. Simulation of electric field distribution of non-metallic shell. (a) Surface electric field distribution. (b) Cross section electric field distribution cloud picture. (c) electric field direction. (d) contour map of electric field distribution

of the shell is aluminum, which can be considered as a unified entity due to the strong contact between the upper and lower shells. The Faraday cage effect demonstrates that the electric field induced inside the shell is equal in magnitude and opposite in direction to the external electric field. Upon superposition, the electric field strength inside the shell will approach 0, as evidenced by the simulation results in FIG. 8. Additionally, it can be observed from the figure that the direction of the magnetic field on the surface of the metal shell is perpendicular to its surface, and that there is no tangential electric field on its surface, consistent with electrostatic shielding phenomenon.

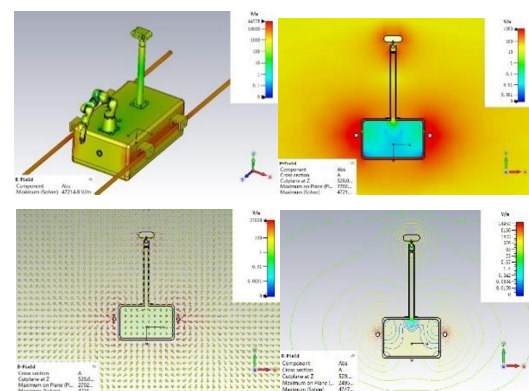


Fig.8. Simulation result of electric field distribution in metal shell

From the simulation results, we have identified a critical point that requires attention. The installation of the camera on a long bracket creates a spatial distance between the camera and the device shell, resulting in a potential difference. If the bracket is constructed from insulating material, there exists a potential difference of approximately 300V between the camera potential and the interior of the main housing. While these two can be connected through a data signal cable to achieve an equal

potential effect, fluctuations in the power grid can still impact signal transmission, leading to image distortion and blurring. This phenomenon also contributes to interference in high-voltage cable image acquisition. Therefore, it is essential for the camera bracket to undergo equipotential processing in order to ensure stability in image signal transmission.

The optimized simulation diagram is depicted in Figure 9 below. The optimized electric field strength of the camera bracket has been reduced from approximately 100V/m to below 5V/m, and the electric field strength at the connection between the shell and the bracket has also been decreased from 50V/m to below 1V/m, thereby achieving a significant shielding effect.

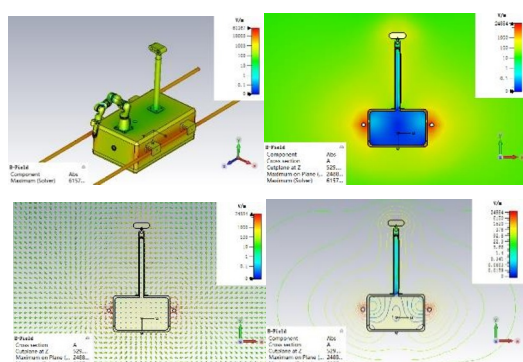


Fig.9. Simulation result of electric field distribution in metal shell after optimization

4 Conclusion

In this paper, the spatial electromagnetic field distribution in the near-field area of the power grid is obtained through numerical calculation. The electromagnetic simulation analysis results are obtained by model simulation analysis. The conventional analog charge method and Biot-Savart method are suitable for solving the electromagnetic field distribution on a two-dimensional plane, but they face challenges in solving the three-dimensional electromagnetic field distribution, particularly the analog charge method which is an approximate equivalent approach. It generally exhibits significant calculation errors in the vicinity of the analog charge and cannot accurately calculate the electric field distribution near potential bodies such as equipment surfaces. The three-dimensional simulation method proposed in this paper effectively addresses these challenges by providing a solution for the three-dimensional electromagnetic field distribution in close proximity to high voltage transmission cables and equipment surfaces.

The analysis results indicate that the selection of shell material and structure design has a significant influence on electric field shielding. When appropriate shielding material is used and optimized design is carried out, an absence elimination device mounted on the power grid can become an equipotential body, thereby achieving good shielding effect. However, due to the complete metal shell, there are certain security risks in the operation and installation of the equipment. In order to

improve safety during operation, the shell of the missing device is made of epoxy material with excellent insulation and mechanical properties. Additionally, the aluminum shielding layer inside the epoxy shell is redesigned, ensuring good electrical contact connection for each part of the device to guarantee its shielding efficiency.

The electric field distribution in cross-section shows relatively high electric field strength near the power grid split line and relatively low strength in middle position. To avoid interference from strong electric fields on core control boards, it is recommended to place them as far as possible from areas with high electric field strength during structural design.

References

1. Leonard B. Loeb, James H. Parker, E. E. Dodd, William N. English; The Choice of Suitable Gap Forms for the Study of Corona Breakdown and the Field Along the Axis of a Hemispherically Capped Cylindrical Point - to - Plane Gap. *Rev. Sci. Instrum.* 1 January 1950; 21 (1) : 42-47. <https://doi.org/10.1063/1.1745419>.
2. Krajewski W. BEM analysis of electric field excited by overhead HV lines erected in built-up areas[J]. *IEE Proceedings-Science, Measurement and Technology*, 1997, 144(2): 81-86.
3. Trlep M, Hamler A, Jesenik M, et al. Electric field distribution under transmission lines dependent on ground surface[J]. *IEEE Transactions on Magnetics*, 2009, 45(3): 1748-1751.
4. Liu Zhenya. *UHV Power grid* [M]. Beijing: China Economic Press, 2005.
5. Liu Qingsong. Research on application of finite-difference Time-domain method in Electromagnetic Field simulation of ultra-high voltage transmission lines [D]. Chongqing University, 2004.
6. Yu Jihui. *Principles of Electromagnetic Field* [M]. Chongqing University Press, 2003.
7. M.S. Abou-Seada, E. Nasser. Digital computer calculation of the electric potential and field of a rod gap[J]. *Proceedings of the IEEE*, 2011, 56(5): 813-820.
8. Wu Xiong, Wan Baoquan. *Electromagnetic Environment of power transmission and transformation project* [M]. Beijing: China Electric Power Press, 2009:15-16.
9. FENG Jian, LUO Il-sung, WANG Feng et al. Analysis of electromagnetic Environment Effect of 110kV transmission line inspection UAV [J]. *Journal of Electric Power*, 2021, 36(06):498-504. DOI:10.13357/j.dlxb.2021.059.
10. WANG Shufeng, LU Tiebing, Cui Xiang. Review of Electromagnetic Compatibility Analysis Methods and Mathematical Models of Power Systems [J]. *Electric Power Information*, 1998, (04):3-7.